Journal of Materials Chemistry C

ROYAL SOCIETY OF CHEMISTRY

PAPER

View Article Online
View Journal | View Issue

Cite this: J. Mater. Chem. C, 2025, 13, 15346

Unveiling the roles of aromaticity in the optoelectronic and charge-transport properties of dehydrobenzo[*n*]annulenes†

Yu Lin,‡[a] Yu Ge,‡[b] Chaojie Xu,‡[a] Haiming Zhang,[a] Chaohua Cui,[b] Yue Wu,*[b] Lifeng Chi*[a] and Qiang Chen*[a]

Dehydrobenzo[*n*]annulenes ([*n*]DBA) are a family of π-conjugated shape-persistent macrocycles, whose properties are governed by both their arylene groups and alkynylene linkages. While diverse members of [*n*]DBAs have been extensively studied, the triacetylene-bridged [24]DBA, a missing member, has remained elusive. Herein, we report the first synthesis of a hexa-*n*-dodecyloxy-substituted [24]DBA using Sonogashira cyclotrimerization of an *in situ* generated triyne intermediate. For comparison, the other three [*n*]DBA derivatives (*n* = 12, 18 and 30) were also synthesized using modified literature procedures. Comprehensive structural characterization by nuclear magnetic resonance (NMR) spectroscopy, high-resolution mass spectrometry and single-crystal X-ray diffraction analysis unambiguously confirms the planar geometry of the [*n*]DBA cores and sheet-like two-dimensional packing in the solid state. This complete series of [*n*]DBA enables an exploration of their ring-size-dependent optoelectronic and charge-transport properties. ^{1}H NMR analysis discloses an alternating behaviour between aromaticity and antiaromaticity with increasing core size. UV-vis absorption and fluorescence measurements also reflect an alternation between broad and narrow energy gaps. Moreover, space-charge-limited current (SCLC) measurements demonstrate that antiaromatic [*n*]DBA (*n* = 12 and 24) derivatives exhibit higher hole mobilities than their aromatic counterparts (*n* = 18 and 30). The successful synthesis of [24]DBA not only fills a critical gap in the [*n*]DBA family, but also establishes a structure–property relationship for designing π-extended [*n*]DBA derivatives with enhanced charge transport.

Received 16th May 2025,
Accepted 17th June 2025

DOI: 10.1039/d5tc01951f

rsc.li/materials-c

Introduction

In the past few decades, the field of organic electronics, which involves the application of π-conjugated organic materials as active components in optoelectronic devices, has expanded and diversified into various sub-directions including organic field-effect transistors (OFETs),[1] organic light-emitting devices (OLEDs)[2] and organic photovoltaics (OPVs).[3] Organic materials are advantageous for characteristics including the feasibility of property tuning through wet-chemistry methods, low energy consumption in production and processing, intrinsic mechanical flexibility, lightweight, *etc.*[4] Amongst various performance parameters of organic semiconductors, charge-carrier mobility is one of the most important for their application in electronic devices.[5] To date, small molecule- and polymer-based semiconductors with high mobility of up to 10 $cm^2 V^{-1} s^{-1}$ have been developed.[6] Despite these achievements in materials science, efforts are still devoted to investigating the structure–performance relationships of established molecular systems to facilitate the design and synthesis of optimal electronic materials, in particular with improved charge-carrier mobility and integrated functionality.

Amongst various types of organic semiconductors, π-conjugated rigid macrocycles have garnered tremendous attention owing to their versatile applications.[7,8] They possess remarkable structural and electronic advantages, including well-defined pore sizes that allow for supramolecular binding with electronically active guests[9] and tunable molecular architectures that enable ordered intermolecular arrangement in the

[a] State Key Laboratory of Bioinspired Interfacial Materials Science, Institute of Functional Nano & Soft Materials (FUNSOM), Soochow University, Suzhou 215123, P. R. China. E-mail: chenqiang@suda.edu.cn
[b] Laboratory of Advanced Optoelectronic Materials, Key Laboratory of Novel Semiconductor-Optoelectronics Materials and Devices, College of Chemistry Chemical Engineering and Materials Science, Soochow University, Suzhou 215123, P. R. China

† Electronic supplementary information (ESI) available. CCDC 2441874–2441877. For ESI and crystallographic data in CIF or other electronic format see DOI: https://doi.org/10.1039/d5tc01951f

‡ These authors contributed equally to this work.

solid state.[10,11] Additionally, they do not possess end groups occurring in linear molecules and are known to trap the charge carriers.[12] Furthermore, their delocalized π-conjugation systems and energetically aligned frontier molecular orbitals offer appealing electronic properties, such as efficient intramolecular charge transfer.[13] All of these features synergistically enhance the ordered arrangement in the solid state, thereby increasing the efficiency of charge injection and transport.[14]

Alkyne-containing shape-persistent macrocycles, such as dehydro[*n*]annulenes ([*n*]DA) and dehydrobenzo[*n*]annulenes ([*n*]DBA),[15–17] where *n* represents the number of π-electrons in the cyclic [*n*]annulene skeleton, have received tremendous attention not only because of their function as model structures for aromaticity studies,[18,19] but also for their intriguing physical properties and self-assembly behaviour. Since Eglinton's pioneering work reporting the preparation of acetylenic [12]DBA (Scheme 1),[20] the smallest member of this series, several larger [*n*]DBA derivatives with various oligo-alkynes as linkages connecting the arylene groups, such as [18]DBA[21] and [30]DBA[22] (Scheme 1), have been synthesized.[23–27] This was based on the well-developed synthetic toolboxes involving Cu-[20,21] or Pd-catalyzed cyclooligomerization of alkyne precursors.[22] Representative examples of [*n*]DBAs have been reported by the groups of Haley,[21,28–31] Tobe[32–35] and Komatsu.[36–38] More recently, Nakamura's group presented the synthesis of a series of novel core-extended DBAs possessing long oligoyne linkages.[23,39,40] Despite these breakthroughs, little has been known about dehydrobenzo[24]annulenes ([24]DBA, Scheme 1), which feature triacetylenic linkages between neighbouring phenyl moieties, hindering systematically studying the size-dependent optoelectronic and electric properties of the [*n*]DBA family.

Studies of DBA have focused on their ring-size-dependent tropicity, self-assembly behavior in solution[41] or on the liquid–solid interface[42–46] and non-linear optical properties.[34,47,48] Other works have targeted the applications of small [*n*]DBAs to synthesize polycyclic aromatic hydrocarbons[49] or porous materials.[41,50,51] Alkyne-containing compounds have also shown potential as active components of organic solar cells and field-effect transistors,[52] with the triple bonds either attached to the terminal or functioning as linkages. However, investigations on charge transport in [*n*]DBAs have been rare and the effects of ring size on the charge mobilities of electrons and holes remain unknown. To the best of our knowledge, there is only one report from Tobe's group,[53] in which a [12]DBA was bridged between two Au electrodes and the conductance of the single molecular junction through two anchors was measured.

Herein, we describe the synthesis of an unprecedented hexa-*n*-dodecyloxy [24]DBA (**DBA-3**) using Sonogashira cyclization of a triynyl-substituted iodobenzene as the key step (Scheme 1). By comparing DBA-*n* analogues of different core sizes, we reveal the alternating behavior of their photophysical and electronic properties with increasing linkage length. Specifically, UV-vis absorption and fluorescence spectra of **DBA-1**/**3** show bathochromic shifts in comparison with hypsochromic shifts for **DBA-2**/**4**. ^{1}H NMR analysis discloses an alternation between aromaticity and antiaromaticity with increasing alkynyl linkage length. The alternating pattern of electronic properties and aromaticity are in overall agreement with that calculated by density functional theory (DFT). A solid state stability test by thermal gravity analysis (TGA) and differential scanning calorimetry (DSC) demonstrates that with increasing core size, the thermal stability decreases significantly, in line with observations made for linear alkyne oligomers, or polyynes.[54] Moreover, the charge-carrier mobilities of DBA-*n* were measured by a space-charge-limited current (SCLC) technique,[55] which revealed higher hole mobilities of antiaromatic DBA-*n* systems compared with their aromatic counterpart. This result highlights the important role of antiaromaticity on improving charge-carrier transport of conjugated macrocycles. We note that prior studies on antiaromatic organic semiconductors with a single molecule type, especially those containing five- or eight-membered carbon rings, have also reported higher charge carrier mobilities.[56]

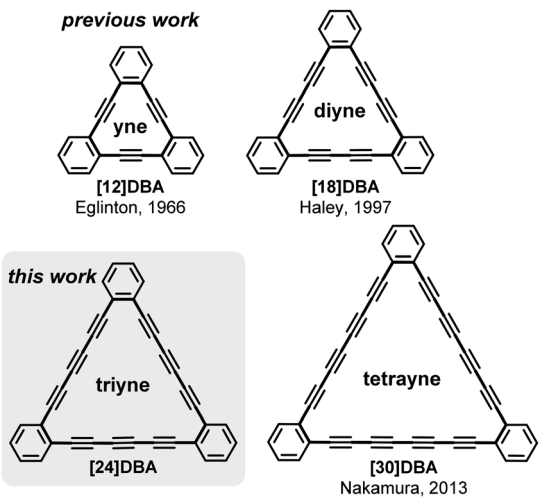

Scheme 1 Chemical structures of the parent [12]DBA,[20] [18]DBA,[21] [24]DBA and [30]DBA.[22]

Results and discussion

Synthesis and characterization of DBA-*n*

The synthetic route towards DBA-*n* is outlined in Scheme 2. *n*-Dodecyl chains are attached to benzene moieties at the vertices of the triangle to maintain high solubility and solution processability. All syntheses started with a previously known 1,2-bis(*n*-dodecyloxy)-4,5-diiodobenzene (**5**),[44] which was obtained in good yield by alkylation and iodination of catechol (see ESI†). **DBA-1** and **DBA-2** were synthesized for comparison adopting a literature-reported procedure with slight modification.[32,45] To start with, Sonogashira coupling of **5** with (triisopropylsilyl)-acetylene (1.4 eq.) afforded mono-(**1**) and bis-fold coupling products (**2**) in 22% and 53% yields, respectively. Next, desilylation of **1** with TBAF at room temperature followed by a Stephens–Castro cyclotrimerization provided **DBA-1** in 29% yield over two steps.[57] After deprotection of **2** with TBAF, the resulting free diyne was

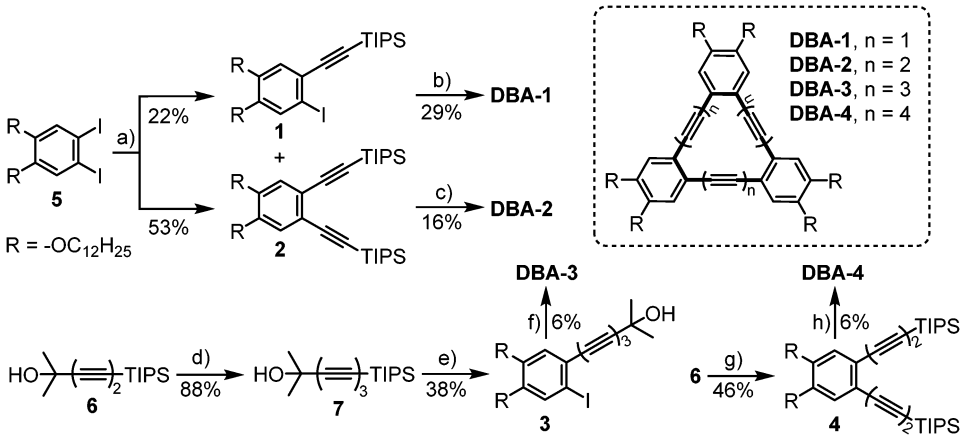

Scheme 2 Synthetic route towards DBA-*n* (*n* = 1–4). Reagents and conditions: (a) (triisopropylsilyl)acetylene, $Pd(PPh_3)_2Cl_2$, CuI, TEA, 40 °C; (b) 1. TBAF, THF, r.t.; 2. CuI, K_2CO_3, DMF, 140 °C; (c) 1. TBAF, THF, r.t.; 2. $Pd(PPh_3)_2Cl_2$, CuI, I_2, i-Pr_2NH, THF, r.t.; (d) 1. TBAF, THF, 0 °C; 2. 1-Bromo-2-(triisopropylsilyl)acetylene, CuCl, *n*-$BuNH_2$, $NH_2OH{\cdot}HCl$, MeOH : H_2O = 2 : 1 (v/v), r.t.; (e) **5**, $Pd(PPh_3)_4$, CuI, TBAF, i-Pr_2NH, THF, r.t.; (f) $Pd(PPh_3)_4$, CuI, KOH, TEBAC, toluene, 65 °C; (g) $Pd(PPh_3)_4$, CuI, KOH, TEBAC, toluene, 80 °C; (h) 1. TBAF, THF, 0 °C; 2. $Pd(PPh_3)_2Cl_2$, CuI, I_2, i-Pr_2NH, THF, r.t. Abbreviations: TEA = triethylamine; TBAF = tetrabutylammonium fluoride; THF = tetrahydrofuran; DMF = *N*,*N*-dimethylformamide; TEBAC = benzyltriethylammonium chloride.

placed under Hay homocoupling conditions to give **DBA-2** in 16% yield. **DBA-3** and **DBA-4** were prepared from a protected butadiyne **6**, which was synthesized in 92% yield by Cadiot–Chodkiewicz cross-coupling of 2-methyl-3-butyn-2-ol and 1-bromo-2-(triisopropylsilyl)acetylene.[58] Desilylation of **6** with TBAF, followed by a second-round cross-coupling, provided triyne **7** in a very good yield of 88%. Then, the key precursor **3** was obtained in 38% yield through *in situ* desilylation of **7** with TBAF, followed by Sonogashira coupling with **5**. Finally, **3** was deprotected with KOH *in situ* to give free triyne, which underwent Sonogashira cyclotrimerization to form **DBA-3** in 6% yield. When butadiyne **7** was deprotected with KOH and coupled with **5** under Sonogashira conditions, precursor **4** could be obtained in 46% yield. Subsequent deprotection of **4** with TBAF afforded free bis-diyne, which underwent Hay coupling to afford **DBA-4** in 6% yield.[22] The relatively low yield of **DBA-3** and **DBA-4** might be due to the low stability of the deprotected triyne and diyne intermediates, especially under basic conditions, as well as their high preference to provide linear oligomeric and polymeric byproducts during the final cyclization step. These DBAs were characterized by a combination of high-resolution matrix-assisted laser desorption/ionization time-of-flight mass spectrometry (MALDI-TOF MS) and nuclear magnetic resonance (NMR) spectroscopy. They are also stable in solution and can be stored for several months under ambient conditions. However, in the solid state, **DBA-4** gradually degraded and was even stored in a deep freezer (−20 °C), probably due to topochemical polymerization of long alkyne linkages in the solid state.[59] This phenomenon has also been reported for a [30]DBA derivative functionalized with shorter alkyl chains that underwent decomposition after storing in the solid state for several months.[22] Solid state TGA revealed high weight loss temperatures (>300 °C for 5% weight loss) for all DBAs (Fig. S15–S18, ESI†). However, DSC analyses show irreversible exothermic reactions in the temperature range of 100–200 °C for all DBAs except for **DBA-1**, with the reaction temperatures decreasing as the alkynyl linkage length increases (Fig. S15–S18, ESI†).

Single-crystal X-ray diffraction analysis and solid-state packing

Single crystals of DBA-*n* suitable for X-ray diffraction analysis were obtained by liquid phase diffusion at room temperature (see ESI,† for details), despite the well-known challenge of crystallizing compounds with long *n*-alkyl chains. Although in the crystal structures, some of the alkyl groups are disordered, the rigid [*n*]DBA cores can still be clearly resolved (Fig. 1a–d). Interestingly, **DBA-1** crystallized as a clathrate with chloroform-*d* molecules having a stoichiometry of 1 : 1. **DBA-1** and the solvent molecules co-assembled to form a two-dimensional sheet-like structure, in which the [12]DBA cores were aligned to the layer plane (Fig. 1e). Inside the layer, the *n*-dodecyl groups and chloroform-*d* molecules occupied the space between [12]DBA, indicating that van der Waals force and DBA–O···Cl–$CDCl_2$ interaction (Fig. S1, ESI†) play vital roles in forming the sheet-like structure. In addition, DBA–O···D–CCl_3 interactions exist between chloroform-*d* and **DBA-1** molecules in the neighboring layer. The other larger DBA-*n* (*n* = 2, 3, 4) crystallized in a similar manner with alkyl chains filling the space between the rigid [*n*]DBA cores and the main difference is that no co-crystallized solvent molecules were observed (Fig. 1f–h). It is interesting to note that the core of **DBA-3** is slightly distorted with an average dihedral angle of 6.0° (defined by ≡C–C=C–C≡), and average C≡C–C angle of 177.3°. The root-mean-square deviation of the [24]DBA core from its mean plane is 0.11 Å. These results indicate that there exist slight ring strains in **DBA-3**, which is expected to make them reactive towards chemical reactions. In the crystals, molecules of **DBA-3** self-assembled into a sheet-like two-dimensional structure with π–π interaction between the triyne linkages and the line-to-line distance is around 3.49 Å.

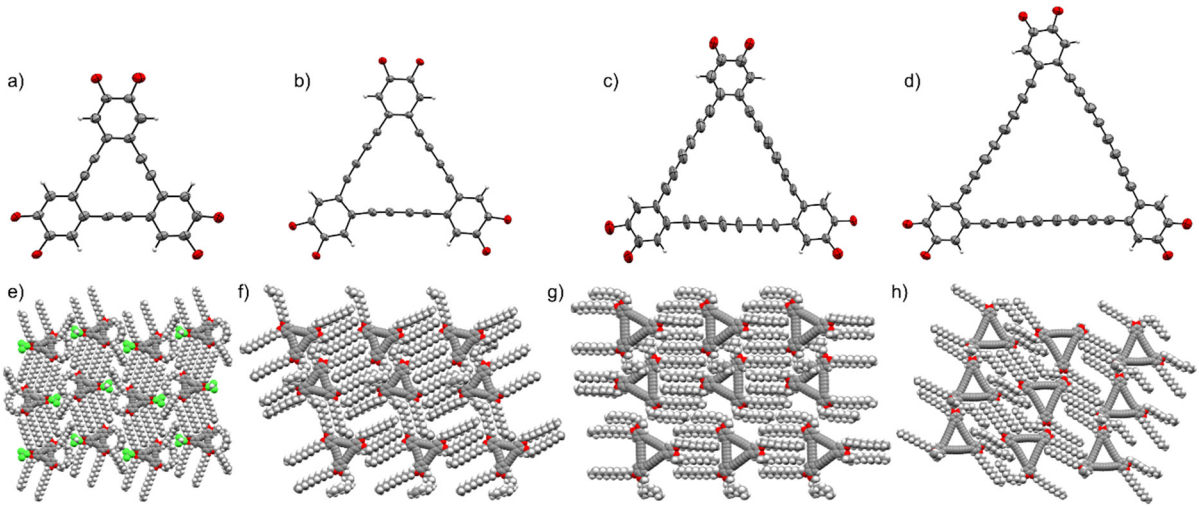

Fig. 1 Single-crystal X-ray structures of DBA-*n*. (a)–(d) ORTEP drawings of **DBA-1** to **DBA-4** with thermal ellipsoids at 50% probability level. *n*-Dodecyl groups are omitted for clarity. (e)–(h) Space-filling models of **DBA-1** to **DBA-4** show two-dimensional sheet-like packing structures in their crystals. Gray = carbon, red = oxygen, green = chloro, white = hydrogen.

The existence of π–π overlap in the solid state implies that **DBA-3** could be potentially used as a semiconductor with high charge-carrier mobility.

Ring-size-dependent alternation between paratropic and diatropic ring current

According to Hückel's rule, cyclic π-conjugated systems possessing $4n$ delocalized π-electrons are antiaromatic, while those with $4n + 2$ electrons are aromatic.[60] The aromaticity of DBA-*n* (n = 1–4) is expected to be dependent on the sizes of their inner dehydro[*n*]annulene rings. ^{1}H NMR spectroscopy and nuclear independent chemical shift (NICS) are experimental and theoretical criteria for determining aromaticity.[61–63] As shown in Fig. 2a, due to the D_{3h} symmetry of DBA-*n*, only a singlet peak appears in the aromatic region of their ^{1}H NMR spectra. The signal of H_b on the periphery of **DBA-1** is located at 6.72 ppm, experiencing an upfield shift by 0.23 ppm relative to H_a on the acyclic precursor **1**. In comparison, the chemical shift value of H_b on **DBA-2** is 0.22 ppm larger than H_a on **2**, reflecting diatropic ring current in the dehydro[18]annulene core. **DBA-3** and **DBA-4** show again upfield and downfield shifts by 0.12 and 0.03 ppm compared with their acyclic precursors, respectively. This phenomenon can be understood in view of the paratropic and diatropic ring currents within the $4n$ and $4n + 2$ π-electron systems, shielding and de-shielding the protons on the phenylene groups (H_b), respectively. Besides, as indicated by the chemical shift difference between H_a and H_b, the induced ring current intensity of DBA-*n* decays with expanding core sizes (Fig. 2c).

NICS(1) calculations of DBA-*n*′, in which the *n*-dodecyl chains of DBA-*n* were replaced by methyl groups, were carried out at the GIAO-B3LYP/6-31G(d,p) level of theory (Fig. S10, ESI†). As demonstrated in Fig. 2c, positive NICS(1) values are observed for **DBA-1**′ and **DBA-3**′, reflecting their paratropic ring current; however, the negative NICS(1) values of **DBA-2**′ and **DBA-4**′ indicate diatropic ring currents associated with the $4n + 2$ π-electrons in their dehydroannulene rings. Moreover, the NICS(1) value of **DBA-3**′ decays to nearly 1/3 of **DBA-1**′ with expansion of the ring size and that of **DBA-4**′ also decays by the same extent compared with **DBA-2**′. The alternation of NICS(1) between positive and negative values with increasing core sizes is consistent with the shielding and de-shielding effect of H_b derived from ^{1}H NMR experiments, and the attenuation of the ring current effect with increasing sizes is in line with that reported by Nakamura *et al.*[22]

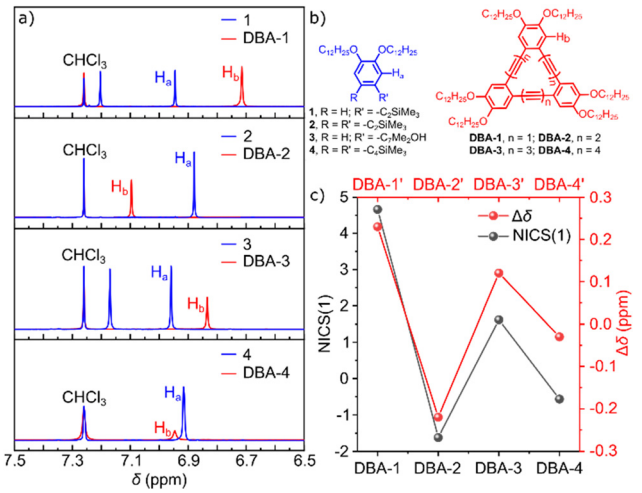

Fig. 2 (a) Comparison of the aromatic region of the ^{1}H NMR spectra of DBA-*n* (from top to bottom n = 1, 2, 3 and 4, respectively) with their corresponding precursors (**1–4**) measured in $CDCl_3$ at 298 K. (b) Chemical structures of **1–4** and DBA-*n* used for the ^{1}H NMR study shown in panel a. (c) Experimental chemical shift changes of H_b with respect to H_a ($\Delta\delta = \delta_a - \delta_b$) and NICS(1) values of the central rings of DBA-*n*′ (*n*-dodecyl groups were replaced by methyl for simplicity), showing alternating behavior between paratropic and diatropic ring currents.

Ring-size-dependent photophysical properties

In order to study the effect of ring size on the optoelectronic properties of DBA-*n*, their UV-vis absorption and fluorescence spectra were measured in chloroform at room temperature. As shown in Fig. 3a, the absorption spectra are dominated by electronic transitions with peaks located at 317 nm, 353 nm, 373 nm and 412 nm, respectively, exhibiting an overall bathochromic shift with extending the length of alkynic linkages. The observable lowest-energy absorption bands are located at 343 nm (1.21×10^4 M^{-1} cm^{-1}), 396 nm (5.22×10^4 M^{-1} cm^{-1}), 447 nm (1.23×10^5 M^{-1} cm^{-1}) and 451 nm (5.59×10^5 M^{-1} cm^{-1}), respectively. The source of these absorption peaks was predicted by time-dependent density functional theory (TD-DFT) calculations as electronic transitions from the ground state (S0) to the second (S2) or higher (S3 and S4) excited states, mainly originating from an admixture of HOMO → LUMO, HOMO−1 → LUMO and HOMO → LUMO+1 transitions (Fig. S6–S9, ESI†).[64] Apparently, the contribution of electronic transition from the ground state to the first excited state (S0–S1) is negligible, which could be accounted for by their near-zero oscillator strengths, indicating that this type of electronic transition is forbidden due to symmetry considerations. According to the onsets of their lowest-energy absorption peaks, the optical energy gaps are calculated to be 2.62 eV, 2.90 eV, 2.64 eV, and 2.66 eV, respectively, showing good agreement with the order of HOMO–LUMO energy gaps calculated by DFT (Fig. 3b and c).

All DBA-*n* show bright (blue to yellow) fluorescence in dilute chloroform solution. As shown in Fig. 3a, their fluorescence spectra differ significantly from each other despite their similar chemical structures. Specifically, the maximum emission wavelength (λ_{em}) of **DBA-1** is located at 557 nm with a fluorescence quantum yield of 0.098; however, that for **DBA-2** is blue-shifted to 460 nm, although the size of the conjugation core seems to be expanded, and its fluorescence quantum yield is significantly increased to 0.34. **DBA-3** exhibits a bathochromic shift compared with **DBA-2**, showing λ_{em} at 554 nm, while that of **DBA-4** shows again a hypochromic shift. The absolute fluorescence quantum yields (Φ) measured for **DBA-3** drop to 0.042, but that of **DBA-4** is too small to be determined accurately. Overall, the fluorescence spectra maxima of **DBA-1**/**3** show a bathochromic shift, while that of **DBA-2**/**4** exhibits a hypsochromic shift. There is thus an alternation behaviour, which is of the same trend as the onset wavelength of their lowest-energy absorption peaks.

Electrochemical properties and charge-carrier mobilities

To study the electrochemical properties of DBA-*n* and evaluate their electron- or hole-injection feasibility, cyclic voltammetry (CV) measurements were carried out (Fig. 4a). The voltammograms measured for DBA-*n* exhibit distinct oxidation processes, while their reduction peaks could not be detected, which is consistent with their electron-rich character. The voltammograms of **DBA-1** and **DBA-3** are characterized by two distinct oxidation waves, while those of aromatic **DBA-2** and **DBA-4** exhibit only one. The experimentally observed irreversibility might be related to instability of the corresponding oxidized

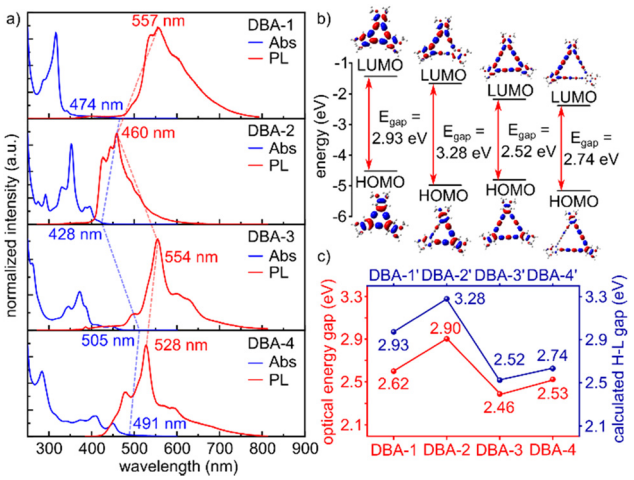

Fig. 3 Ring-size-dependent optoelectronic properties of the DBA-*n* series. (a) UV-vis absorption and fluorescence spectra of DBA-*n* (*n* = 1–4) measured in chloroform ($c = 10^{-6}$ M) at room temperature. The red dashed lines follow the emission maxima and the blue dashed lines follow the onsets of their lowest-energy absorption band, showing the same oscillatory trend. (b) Density functional theory calculated frontier molecular orbitals of the DBA-*n* series (B3LYP/6-31G(d,p)) and their HOMO–LUMO energy gaps (from left to right, *n* = 1, 2, 3 and 4, respectively). (c) Optical energy gaps derived from UV-*vis* absorption and DFT-calculated HOMO–LUMO energy gaps of the DBA-*n* series showing alternating trends of energy gaps with increasing core sizes.

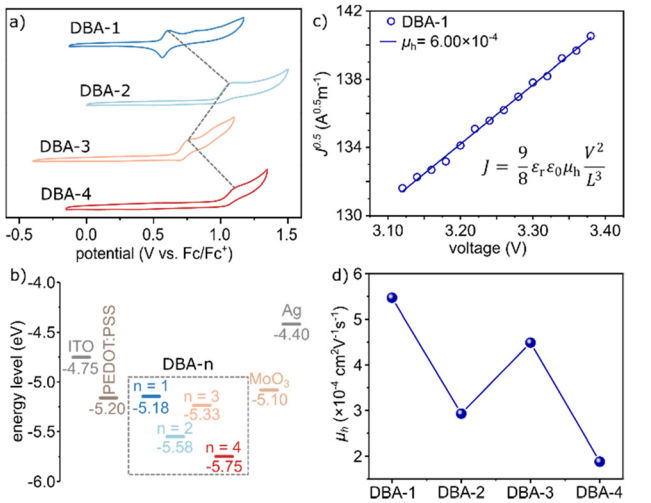

Fig. 4 Electrochemical properties and charge carrier mobilities of DBA-*n*. (a) Cyclic voltammogram of DBA-*n* measured in dichloromethane with 0.4 M *n*-Bu_4N PF_6 as the electrolyte at room temperature (c = 1.0 mM, scan rate = 100 mV s^{-1}). The grey dashed traces follow the peak potentials of the first oxidation waves, respectively. (b) HOMO energy levels of DBA-*n* (HOMO = $-(4.8 + E_{ox}^{onset} - E_{Fc}^{onset})$ eV) and work function of the electrode materials referred to the vacuum level, indicating their energy level matching. (c) Typical current/applied voltage curve for the spin-coated **DBA-1** film (114 nm thick) placed between ITO and Ag/MoO_3 electrodes. The circles represent experimental data and the lines reflect a linear relationship between square root of current and voltage in the experimental region. (d) Ring-size dependency of hole-mobilities of the DBA-*n* series, showing the same alternating trend with their HOMO energy levels.

cationic species.[22] The first oxidation potentials of **DBA-1** and **DBA-3** are relatively lower than their aromatic analogues, reflecting their higher HOMO levels. Moreover, two-electron oxidation of **DBA-1** and **DBA-3** results in the emergence of aromatic π-systems with high stabilization energy, which makes their further oxidation difficult. Their electrochemical HOMO energies referred to the vacuum level could be estimated from the CV measurement, showing higher values for **DBA-1**/**3** than **DBA-2**/**4**, in excellent agreement with the DFT calculations (Fig. 4b).

Due to the absence of efficient electron accepting capability of DBA-*n*, as reflected by the CV measurement, their hole mobilities (μ_h) were investigated using the space-charge-limited current (SCLC) technique.[55] Hole-only devices with a structure of glass/ITO/PEDOT:PSS/active layer/MoO_3/Ag were fabricated and measured, in which the barrier height between the DBA-*n* and electrodes (MoO_3/Ag) was reduced to form ohmic contact (Fig. 4b). The energy level matching is essential to minimize interfacial barriers, thus ensuring reliable determination of the charge transport properties through the current–voltage characteristics analysis. In this work, current–voltage sweeps were performed in the dark from −5.0 V to 5.0 V for all devices. The μ_h values of DBA-*n* were derived from the SCLC expression described by the original Mott–Gurney equation:[65]

$$J = \frac{9}{8}\varepsilon_r\varepsilon_0\mu_h\frac{V^2}{L^3}$$

where $\varepsilon_r \approx 3$ is the relative permittivity of the samples, ε_0 is the permittivity of the free space, μ_h is the charge carrier mobility, J is the measured dark current density, V is the applied voltage, and L is the thickness of the sample film. A typical square root plot of measured current density (J) *versus* applied voltage (V) for **DBA-1** is shown in Fig. 4c. Using this method, the hole mobilities (μ_h) of DBA-*n* (n = 1, 2, 3 and 4) were determined to be 5.47×10^{-4} cm^2 V^{-1} s^{-1}, 2.93×10^{-4} cm^2 V^{-1} s^{-1}, 4.49×10^{-4} cm^2 V^{-1} s^{-1} and 1.88×10^{-4} cm^2 V^{-1} s^{-1}, respectively (Fig. 4d), by averaging two independent measurements (Fig. S12 and S13, ESI†). The hole mobility of **DBA-1**/**3** is higher than that of the aromatic **DBA-2**/**4**. The alternating pattern of μ_h between high and low mobility values is similar to the order of their HOMO levels, which is related to the aromaticity or antiaromaticity of the dehydro[*n*]annulene rings. This result thus manifests the advantage of including antiaromatic cores over aromatic ones for designing high mobility organic semiconductors.

To further understand the mechanism of enhanced hole mobility of antiaromatic DBAs, their packing structures in the solid state were analysed by UV-vis absorption spectroscopy and X-ray diffraction (XRD). The UV-vis absorption spectra of dip-coated films of all DBAs showed significant spectral broadening and red-shifts (~10 nm) of the main peaks compared with that measured in chloroform (Fig. S10, ESI†). These observations reflect the existence of π–π stacking in the films of all DBAs, which facilitates charge transport. X-Ray diffraction (XRD) analyses of the thin films reveal distinct structural differences: antiaromatic **DBA-1**/**3** displays a more ordered crystalline structure, while the aromatic **DBA-2**/**4** shows expanded interlayer spacing and amorphous or nanocrystalline character (Fig. S14, ESI†). These results indicate that the HOMO levels, interlayer packing and crystallinity collectively enhance the hole mobility of antiaromatic DBAs.

Conclusions

In conclusion, the syntheses of a series of triangular DBA-*n* (n = 1–4) with varying core sizes have been accomplished. In particular, **DBA-3** featuring a hexatriyne linkage between the benzene moieties was synthesized for the first time employing a Sonogashira cyclotrimerization reaction. Single-crystal X-ray diffraction analysis not only unambiguously proved their molecular structures, but also revealed their sheet-like two-dimensional packing in the solid state stabilized by van der Waals forces between the alkyl chains and weak π–π interaction between the alkyne linkers in the neighboring layers. Optoelectronic and charge mobility properties could thus be elucidated as a function of their ring sizes. Combined ^{1}H NMR and NICS(1) analysis demonstrated an alternation between aromatic and antiaromatic ring currents across the DBA-*n* series, with the odd-numbered DBA-*n* exhibiting paratropic ring current (antiaromatic) and even-numbered counterparts displaying diatropic ring current (aromatic). The same alternating trend was also manifested in their optical properties: UV-*vis* absorption and fluorescence spectra displayed bathochromic shifts for **DBA-1**/**3** and hypsochromic shift for **DBA-2**/**4**. Furthermore, charge-carrier mobility measurements *via* the SCLC method revealed an aromaticity-dependent behaviour, with the antiaromatic **DBA-1**/**3** having superior hole mobility (*e.g.*, 5.47×10^{-4} cm^2 V^{-1} s^{-1} and 4.49×10^{-4} cm^2 V^{-1} s^{-1}, respectively) compared to the aromatic **DBA-2**/**4**, also attributed to the relatively higher HOMO levels (as corroborated by cyclic voltammetry) of **DBA-1**/**3** allowing for effective hole injection. These results thus highlight the importance of including an antiaromatic framework for designing high charge-carrier mobility organic semiconductors, challenging the traditional focus on purely aromatic systems. We envision that the synthetic strategy disclosed here will find applications in constructing other larger alkyne-based macrocycles and the structure–property relationships elucidated in this work will provide crucial insights for tailoring the charge transport properties of macrocycles by controlling the conjugation pathway and aromaticity.

Author contributions

Q. C., L. C. and Y. W. conceived the project. Y. L. performed the synthesis, characterization and photophysical property investigation of all compounds under the supervision of Q. C. and C. X. Y. G. conducted SCLC measurements under the supervision of Y. W. and C. C. Q. C. and Y. W. prepared the manuscript. All authors discussed the results, and reviewed and commented on the manuscript.

Conflicts of interest

The authors declare no conflicts of interest.

Data availability

The data supporting the findings of this article have been included as part of the ESI.†

Acknowledgements

This work was financially supported by the National Natural Science Foundation of China (22405187, U24A20496), the Natural Science Foundation of Jiangsu Province (BK20240759), the Gusu Innovation and Entrepreneurship Leading Talent Program (ZXL2024391), the Collaborative Innovation Center of Suzhou Nano Science & Technology, the 111 Project, Suzhou Key Laboratory of Surface and Interface Intelligent Matter (No. SZS2022011), the Gusu Innovation and Entrepreneurship Talent Program Major Innovation Team (ZXD2023002), and the Innovative Center for Molecular Science of Surface and Interface (MOSSI), Soochow University.

Notes and references

1 D. Braga and G. Horowitz, *Adv. Mater.*, 2009, **21**, 1473–1486.
2 G. Hong, X. Gan, C. Leonhardt, Z. Zhang, J. Seibert, J. M. Busch and S. Bräse, *Adv. Mater.*, 2021, **33**, 2005630.
3 L. X. Chen, *ACS Energy Lett.*, 2019, **4**, 2537–2539.
4 M. Sawatzki-Park, S.-J. Wang, H. Kleemann and K. Leo, *Chem. Rev.*, 2023, **123**, 8232–8250.
5 V. Coropceanu, J. Cornil, D. A. da Silva Filho, Y. Olivier, R. Silbey and J.-L. Brédas, *Chem. Rev.*, 2007, **107**, 926–952.
6 G. Schweicher, G. Garbay, R. Jouclas, F. Vibert, F. Devaux and Y. H. Geerts, *Adv. Mater.*, 2020, **32**, 1905909.
7 C. Li, C. Wang, Y. T. Guo, Y. Z. Jin, N. N. Yao, Y. G. Wu, F. L. Zhang and W. W. Li, *J. Mater. Chem. C*, 2019, **7**, 3802–3810.
8 M. Ball, B. Zhang, Y. Zhong, B. Fowler, S. Xiao, F. Ng, M. Steigerwald and C. Nuckolls, *Acc. Chem. Res.*, 2019, **52**, 1068–1078.
9 B. Li, G. P. A. Yap, V. St-Onge, N. Mavragani, T. T. H. Dao, P. Baillargeon, P. Fournier, Y. L. Dory and J. P. Claverie, *ACS Mater. Lett.*, 2024, **6**, 1288–1296.
10 S. E. Lewis, *Chem. Soc. Rev.*, 2015, **44**, 2221–2304.
11 J. Xia and R. Jasti, *Angew. Chem.*, 2012, **124**, 2524–2526.
12 S. S. Zade and M. Bendikov, *J. Org. Chem.*, 2006, **71**, 2972–2981.
13 S. Zhong, L. Zhu, S. Wu, Y. Li and M. Lin, *Chin. Chem. Lett.*, 2023, **34**, 108124.
14 X.-K. Chen, L.-Y. Zou, S. Huang, C.-G. Min, A.-M. Ren, J.-K. Feng and C.-C. Sun, *Org. Electron.*, 2011, **12**, 1198–1210.
15 E. L. Spitler, C. A. Johnson and M. M. Haley, *Chem. Rev.*, 2006, **106**, 5344–5386.
16 F. Sondheimer, R. Wolovsky, P. J. Garratt and I. C. Calder, *J. Am. Chem. Soc.*, 1966, **88**, 2610.
17 J. A. Marsden, G. J. Palmer and M. M. Haley, *Eur. J. Org. Chem.*, 2003, 2355–2369.
18 J. Jusélius and D. Sundholm, *Phys. Chem. Chem. Phys.*, 2001, **3**, 2433–2437.
19 E. Kleinpeter and A. Koch, *Tetrahedron*, 2013, **69**, 1481–1488.
20 I. D. Campbell, G. Eglinton, W. Henderson and R. A. Raphael, *Chem. Commun.*, 1966, 87–89.
21 M. M. Haley, S. C. Brand and J. J. Pak, *Angew. Chem., Int. Ed. Engl.*, 1997, **36**, 836–838.
22 S.-i Kato, N. Takahashi and Y. Nakamura, *J. Org. Chem.*, 2013, **78**, 7658–7663.
23 S. i Kato, N. Takahashi, H. Tanaka, A. Kobayashi, T. Yoshihara, S. Tobita, T. Yamanobe, H. Uehara and Y. Nakamura, *Chem. – Eur. J.*, 2013, **19**, 12138–12151.
24 E. M. García-Frutos, F. Fernández-Lázaro, E. M. Maya, P. Vázquez and T. Torres, *J. Org. Chem.*, 2000, **65**, 6841–6846.
25 N. Saito, R. Terakawa and M. Yamaguchi, *Chem. – Eur. J.*, 2014, **20**, 5601–5607.
26 S. Maier, N. Hippchen, F. Rominger, J. Freudenberg and U. H. F. Bunz, *Chem. – Eur. J.*, 2021, **27**, 16320–16324.
27 Y. Ohtomo, K. Ishiwata, S. Hashimoto, T. Kuroiwa and K. Tahara, *J. Org. Chem.*, 2021, **86**, 13198–13211.
28 J. J. Pak, T. J. R. Weakley and M. M. Haley, *J. Am. Chem. Soc.*, 1999, **121**, 8182–8192.
29 D. B. Kimball, M. M. Haley, R. H. Mitchell, T. R. Ward, S. Bandyopadhyay, R. V. Williams and J. R. Armantrout, *J. Org. Chem.*, 2002, **67**, 8798–8811.
30 W. B. Wan, D. B. Kimball and M. M. Haley, *Tetrahedron Lett.*, 1998, **39**, 6795–6798.
31 M. L. Bell, R. C. Chiechi, C. A. Johnson, D. B. Kimball, A. J. Matzger, W. Brad Wan, T. J. R. Weakley and M. M. Haley, *Tetrahedron*, 2001, **57**, 3507–3520.
32 K. Tahara, C. A. Johnson, T. Fujita, M. Sonoda, F. C. De Schryver, S. De Feyter, M. M. Haley and Y. Tobe, *Langmuir*, 2007, **23**, 10190–10197.
33 K. Tahara, T. Fujita, M. Sonoda, M. Shiro and Y. Tobe, *J. Am. Chem. Soc.*, 2008, **130**, 14339–14345.
34 K. Tahara, Y. Yamamoto, D. E. Gross, H. Kozuma, Y. Arikuma, K. Ohta, Y. Koizumi, Y. Gao, Y. Shimizu, S. Seki, K. Kamada, J. S. Moore and Y. Tobe, *Chem. – Eur. J.*, 2013, **19**, 11251–11260.
35 K. Tahara, H. Kozuma, V. Venkatesh, E. Ryomura, H. Miyoshi, K. Nakamachi, R. Kishi, H. Takahashi, M. Nakano and Y. Tobe, *ChemPlusChem*, 2017, **82**, 1052–1056.
36 T. Nishinaga, T. Kawamura and K. Komatsu, *J. Org. Chem.*, 1997, **62**, 5354–5362.
37 T. Nishinaga, N. Nodera, Y. Miyata and K. Komatsu, *J. Org. Chem.*, 2002, **67**, 6091–6096.
38 T. Nishinaga, Y. Miyata, N. Nodera and K. Komatsu, *Tetrahedron*, 2004, **60**, 3375–3382.
39 N. Takahashi, S.-i Kato, M. Yamaji, M. Ueno, R. Iwabuchi, Y. Shimizu, M. Nitani, Y. Ie, Y. Aso, T. Yamanobe, H. Uehara and Y. Nakamura, *J. Org. Chem.*, 2017, **82**, 8882–8896.
40 S.-i Kato, R. Kumagai, T. Abe, C. Higuchi, Y. Shiota, K. Yoshizawa, N. Takahashi, K. Yamamoto, M. Z. Hossain, K. Hayashi, T. Hirose and Y. Nakamura, *Chem. Commun.*, 2021, **57**, 576–579.

41 I. Hisaki, S. Nakagawa, N. Ikenaka, Y. Imamura, M. Katouda, M. Tashiro, H. Tsuchida, T. Ogoshi, H. Sato, N. Tohnai and M. Miyata, *J. Am. Chem. Soc.*, 2016, **138**, 6617–6628.
42 Y. Tobe, K. Tahara and S. De Feyter, *Bull. Chem. Soc. Jpn.*, 2016, **89**, 1277–1306.
43 K. Tahara, R. Nakayama, M. Maeda, S. De Feyter and Y. Tobe, *J. Phys. Chem. C*, 2019, **123**, 27020–27029.
44 K. Tahara, K. Nakatani, K. Iritani, S. De Feyter and Y. Tobe, *ACS Nano*, 2016, **10**, 2113–2120.
45 K. Tahara, S. Furukawa, H. Uji-i, T. Uchino, T. Ichikawa, J. Zhang, W. Mamdouh, M. Sonoda, F. C. De Schryver, S. De Feyter and Y. Tobe, *J. Am. Chem. Soc.*, 2006, **128**, 16613–16625.
46 S. Lei, K. Tahara, F. C. De Schryver, M. Van der Auweraer, Y. Tobe and S. De Feyter, *Angew. Chem., Int. Ed.*, 2008, **47**, 2964–2968.
47 K. Kamada, L. Antonov, S. Yamada, K. Ohta, T. Yoshimura, K. Tahara, A. Inaba, M. Sonoda and Y. Tobe, *Chem. Phys. Chem.*, 2007, **8**, 2671–2677.
48 X. Zhou, A.-M. Ren, J.-K. Feng and X.-J. Liu, *Can. J. Chem.*, 2004, **82**, 1172–1178.
49 S. Kawai, V. Haapasilta, B. D. Lindner, K. Tahara, P. Spijker, J. A. Buitendijk, R. Pawlak, T. Meier, Y. Tobe, A. S. Foster and E. Meyer, *Nat. Commun.*, 2016, 7.
50 J. W. Crowe, L. A. Baldwin and P. L. McGrier, *J. Am. Chem. Soc.*, 2016, **138**, 10120–10123.
51 M. Kobayashi, H. Kubo, R. Oketani and I. Hisaki, *CrystEngComm*, 2022, **24**, 5036–5040.
52 C. D. Sheraw, T. N. Jackson, D. L. Eaton and J. E. Anthony, *Adv. Mater.*, 2003, **15**, 2009–2011.
53 M. Kiguchi, K. Tahara, Y. Takahashi, K. Hasui and Y. Tobe, *Chem. Lett.*, 2010, **39**, 788–789.
54 W. A. Chalifoux and R. R. Tykwinski, *Nat. Chem.*, 2010, **2**, 967–971.
55 P. W. M. Blom and M. C. J. M. Vissenberg, *Phys. Rev. Lett.*, 1998, **80**, 3819–3822.
56 T. Nishinaga, T. Ohmae, K. Aita, M. Takase, M. Iyoda, T. Arai and Y. Kunugi, *Chem. Commun.*, 2013, **49**, 5354–5356.
57 R. D. Stephens and C. E. Castro, *J. Org. Chem.*, 1963, **28**, 3313–3315.
58 U. Orcel and J. Waser, *Angew. Chem., Int. Ed.*, 2015, **54**, 5250–5254.
59 T. Li, S. Okada and H. Nakanishi, *Polym. Bull.*, 2003, **51**, 103–109.
60 M. Solà, *Nat. Chem.*, 2022, **14**, 585–590.
61 Z. Chen, C. S. Wannere, C. Corminboeuf, R. Puchta and P. V. R. Schleyer, *Chem. Rev.*, 2005, **105**, 3842–3888.
62 L. M. Jackman, F. Sondheimer, Y. Amiel, D. A. Ben-Efraim, Y. Gaoni, R. Wolovsky and A. A. Bothner-By, *J. Am. Chem. Soc.*, 1962, **84**, 4307–4312.
63 A. J. Matzger and K. P. C. Vollhardt, *Tetrahedron Lett.*, 1998, **39**, 6791–6794.
64 E. Gomez, M. Gutiérrez, M. Moreno, I. Hisaki, S. Nakagawa and A. Douhal, *Phys. Chem. Chem. Phys.*, 2018, **20**, 7415–7427.
65 M. A. Lampert and P. A. Mark, *Current injection in solids*, Academic Press, New York, 1970.